Monthly Notices
of the
ROYAL ASTRONOMICAL SOCIETY

MNRAS **472,** 4013–4023 (2017) doi:10.1093/mnras/stx2246
Advance Access publication 2017 September 5

On the relation between the mass of Compact Massive Objects and their host galaxies

R. Capuzzo-Dolcetta[1]★ and I. Tosta e Melo[1,2]★

[1]*Department of Physics, Sapienza, Università di Roma, P.le A. Moro 5, I-00185 Rome, Italy*
[2]*CAPES Foundation, Ministry of Education of Brazil, DF 70040-020, Brasilia, Brazil*

Accepted 2017 August 28. Received 2017 August 28; in original form 2017 May 12

ABSTRACT

Supermassive black holes and/or very dense stellar clusters are found in the central regions of galaxies. Nuclear star clusters (NSCs) are present mainly in faint galaxies, while supermassive black holes are common in galaxies with masses $\geq 10^{10}$ $M_\odot$. In the intermediate galactic mass range, both types of compact massive objects (CMOs) are found. Here, we present our collection of a huge set of NSC and massive black hole data that enlarges significantly already existing data bases useful to investigate for correlations of their absolute magnitudes, velocity dispersions and masses with structural parameters of their host galaxies. In particular, we directed our attention to some differences between the correlations of NSCs and massive black holes as subsets of CMOs with hosting galaxies. In this context, the mass–velocity dispersion relation plays a relevant role because it seems the one that shows a clearer difference between the supermassive black holes and NSCs. The $M_{\rm MBH}$–σ has a slope of 5.19 ± 0.28, while $M_{\rm NSC}$–σ has the much smaller slope of 1.84 ± 0.64. The slopes of the CMO mass-host galaxy B magnitude of the two types of CMOs are indistinguishable within the errors, while that of the NSC mass–host galaxy mass relation is significantly smaller than for supermassive black holes. Another important result is the clear depauperation of the NSC population in bright galaxy hosts, which reflects also in a clear flattening of the NSC mass versus host galaxy mass at high host masses.

Key words: surveys – galaxies: nuclei – quasars: supermassive black holes.

1 INTRODUCTION

The link between the formation and evolution of galaxies and those of their central region is a debated topic. Various studies suggest that massive galaxies, both elliptical and spiral, harbour a supermassive black hole (SMBH) in their centres, with masses between 10^4 and 10^9 $M_\odot$ (Baldassare et al. 2015 Graham, Ciambur & Soria 2016). The SMBH masses correlate with various properties of their host galaxies, such as the bulge luminosity (Kormendy & Richstone 1995), mass (Häring & Rix 2004), velocity dispersion (Ferrarese & Merritt 2000) and light profile concentration (Gebhardt et al. 2000;Böker et al. 2001 Graham et al. 2001).

Galaxies across the entire Hubble sequence also show the presence of massive and compact stellar clusters referred to as nuclear star clusters (NSCs). NSCs can be up to 4 mag brighter than an ordinary globular cluster (GC), very massive (up to few 10^7 $M_\odot$), and very dense systems, with half-light radius of 2–5 pc. Actually, they are the densest stellar aggregates observed so far (Neumayer 2012). In elliptical galaxies, the NSCs are also referred to as resolved stellar nuclei, but for the sake of simplicity in this paper we will refer all of them simply as NSCs.

The NSCs contain a predominant old stellar population (age $>$ 1 Gyr) and, in many cases, show also the presence of a young stellar population (age $<$ 100 Myr, Böker et al. 2001 Rossa et al. 2006; Carson et al. 2015).

Ferrarese et al. (2006a) and Wehner & Harris (2006) showed that these two types of objects (SMBHs and NSCs) follow somewhat similar correlations with their host galaxy, suggesting they can be considered members of the same family of Compact Massive Objects (CMOs) whose main difference is the mass and the concentration. Note that Balcells et al. (2003) and Graham & Guzmán (2003) were the first to quantify a correlation between the nuclear component and host luminosity.

Kormendy & McClure (1993) and Graham & Spitler (2009) showed that, despite their different morphologies, some galaxies of the Local Group present an NSC, an MBH or both.

Ferrarese et al. (2006b) found a separation in mass between galaxies that host an NSC (those with $M_{\rm g} \lesssim 5 \times 10^9$ $M_\odot$) and those

★ E-mail: roberto.capuzzodolcetta@uniroma1.it (RC-D); iara.tostaemelo@gmail.com (ITeM)

hosting an SMBH (with $M_g \gtrsim 5 \times 10^9$ M$_\odot$). In the transition zone, i.e. in galaxies with mass between 10^8 and 10^{10} M$_\odot$, there are cases where NSCs and SMBHs coexist (Seth et al. 2008; Graham 2012). A good example is the Milky Way (MW), where a 4×10^6 M$_\odot$ black hole coexists with an NSC with $M_{\rm NSC} \approx 1.5 \times 10^7$ M$_\odot$ (Schödel, Merritt & Eckart 2009).

Ferrarese et al. (2006a) showed that the NSC mass versus the host galaxy velocity dispersion (σ) relation is roughly the same observed for SMBHs. On the other hand, Graham (2012) claimed, instead, that the $M_{\rm NSC}$–σ relation is shallower for NSCs ($M_{\rm NSC} \propto \sigma^{1.5}$) than for SMBHs.

Work by Erwin & Gadotti (2012) shows that NSC masses correlate better with bulge masses, while for MBH, there is a closer correlation when considering their masses and their host galaxy total masses. Actually, this result relies on somewhat uncertain determinations of the bulge masses, as discussed by Savorgnan & Graham (2016) which lead to more reliable SMBH versus host mass correlation in Savorgnan et al. (2016).

Some studies also showed that some active galactic nuclei (AGNs) masses relate better with some of their galaxies properties, such as stellar velocity dispersion, $M_{\rm MBH}$–σ_* relation (Greene & Ho 2006) and the galaxy stellar bulge mass, $M_{\rm MBH}$–$M_{\rm gal}$ relation (Peng 2007).

In such a framework, the general scope of this paper is to collect from the literature, the most quantitatively wide data set to improve the knowledge of scaling relations among CMO properties and those of their galactic hosts.

In this context, we directed our attention to the study of the differences between the SMBH mass and the NSC mass versus σ relation, which can be interpreted in term of the migratory explanation for NSC formation.

The paper is organized as follows: Section 2 presents the data base used for building our sample and the methodology. The results and their discussion are presented in Section 3, while Section 4 gives a summary and conclusions.

2 THE DATA BASE

In this paper, we gathered the largest possible set of NSCs, MBHs and AGNs together with their host galaxies properties available in the literature, totalizing more than 700 CMOs, as summarized in Table 1.

2.1 ACS Fornax Cluster Survey

Turner et al. (2012) selected 43 galaxies of the Fornax Cluster with early-type morphologies (E, S0, SB0, dE, dE,N, or dS0,N), using the *F*475*W* and *F*850*LP* bandpasses of the *Hubble Space Telescope* (*HST*) Advanced Camera for Survey (ACSFCS). In 31 galaxies out of 43, representing 72 per cent of the sample, there is a clear stellar nucleus, and the majority of the nuclei are bluer than their host galaxy. The authors provide two apparent magnitudes for the nuclei, in the g and z bands. In this work, we used the g-band values, because the level of nucleation is slightly larger in this band. Note that in Fornax Cluster, the galaxy FCC 21, Fornax A, has an AGN in its centre (Nowak et al. 2008) and FCC 213 has a well-measured BH (Scott & Graham 2013). We will refer to the data for Fornax as FCS.

2.2 ACS Virgo Cluster Survey

Côté et al. (2006) analysed the nuclei of a sample of 100 early-type galaxies in the Virgo cluster, of morphological types E, S0, dE, dEN and dS0, containing either NSCs, MBHs, or both. The images were taken with the ACS instrument in the Wide Field Channel (WFC) using (like in the case of the Fornax galaxies) a combination of the *F*475*W* and *F*850*LP* filters, roughly equivalent to the g and z bands. According to these authors, nucleated galaxies are more concentrated towards the centre of Virgo cluster and some nuclei of ACS Virgo Cluster Survey (ACSVCS) are bluer than the parent galaxy and a central excess is more apparent in the g band rather than in the redder bandpass (Côté et al. 2006). 32 galaxies out of 100 in this sample had their BH masses measured (Gallo et al. 2008), but just 6 of out these 32 were classified as AGN (Côté et al. 2006). We will refer to these data as VCS.

2.3 ACS Coma Cluster Survey

den Brok et al. (2014) analysed the light profile of 200 early-type dwarf galaxies with magnitudes $16.0 \leq m \leq 22.6$ (in the *F*814*W* band) using the *HST*/ACS Coma Cluster Survey (CCS). NSCs are detected in 80 per cent of the galaxies and the authors did not estimate the black holes masses and/or the AGN classification due to the low mass of the early-type galaxies in this sample. The authors confirmed in such work that the NSC luminosity detection fraction decreases strongly towards faint magnitudes. We will refer to these data as CCS.

Table 1. Summary of information about our data sample. First column: sub-sample acronym; second column: sub-sample reference; third column: number of objects; fourth column: types of objects; Columns from fifth to eighth give the minimum and maximum relative errors of the CMO masses and of the host galaxy absolute integrated B magnitude, velocity dispersion and mass. The errors for the Fornax Cluster galaxies $M_{\rm B}$ and for the Coma Cluster galaxies σ were not available from the data sources. The references for the second column are: R1: Turner et al. (2012), R2: Côté et al. (2006), R3: Gallo et al. (2008), R4: den Brok et al. (2014), R5: Matković & Guzmán (2005), R6: Weinzirl et al. (2014), R7: Georgiev & Böker (2014), R8: Peterson et al. (2004), R9: Ferrarese & Ford (2005), R10: Hu (2008), R11: Graham et al. (2011), R12: Scott & Graham (2013), R13: Savorgnan & Graham (2015).

Sample	Ref.	N	CMO type	$M_{\rm CMO}$	$M_{\rm B}$	σ	$M_{\rm g}$
FCS	R1	41	NSC	0.15 – 1.32	–	0.013–0.407	0.02–0.63
FCS	R1	2	BH+AGN	0.41 – 0.53	–	0.014–0.018	0.04–0.108
VCS	R2	68	NSC	0.073 – 0.174	0.002–0.017	0.009–0.53	0.018–1.07
VCS	R3	32	BH+AGN	0.031 – 0.630	0.002–0.007	0.022–0.206	0.006–1.44
CCS	R4–R6	200	NSC	0.04 – 0.75	9.9×10^{-5}–8.0×10^{-3}	–	0.105–1.02
HST	R7	220	NSC	0.138 – 0.294	0.005–0.017	0.029–0.511	0.027–0.294
HST	R7	8	AGN	0.130 – 0.148	0.005–0.006	0.046–0.272	0.094–1.112
MBH	R8–R13	135	BH+AGN	0.013 – 1.54	0.007–0.024	0.025–0.34	0.42–0.64

2.4 *HST* /WFPC2 archive

Georgiev & Böker (2014) presented the properties of 228 NSCs in nearby late-type galaxies observed with the WFPC2/*HST*, in the *B* and *I* bands, with distance modulus ≤33 mag, i.e. distance ≤40 Mpc. To build the sample, the authors avoided the most luminous bulges and all AGNs because their presence would complicate the NSC characterization, but due to technical issues, a few weak AGNs ended up in the sample (8 out of 228). They also concluded that most NSCs in this sample have sizes similar to their possible GCs progenitors, but also that the largest and brightest NSCs reside in the size–luminosity plane between Ultra Compact Dwarf and the nuclei of early-type galaxies. We will refer to these data as *HST*.

2.5 Massive black holes sample

To build our final data set, we collected 127 galaxies for which a dynamical detection of their central black hole mass is available in the literature. We took and interpolated the information of the black hole and its host galaxies given in several catalogues presented by Peterson et al. (2004), Ferrarese & Ford (2005), Hu (2008), Graham et al. (2011), Scott & Graham (2013) and Savorgnan & Graham (2015). It is important to note here the coincidence between some of those 127 objects with some already present in the previous samples: 2 objects from FCS and 23 objects from VCS. Together with eight AGNs that ended up in the *HST*/WFPC2 archive sample, we completed our final MBH sample, totalizing more than 130 BHs and AGNs. We will refer to these data as MBH.

In Table 1, we give a summary of our data base. Our data are available in digital form upon request to the authors.

3 METHOD

Our first aim was to estimate CMO masses for each catalogue presented above and compare such values with the directly observed or derived parameters (absolute *B* magnitude, mass and velocity dispersion) of their host galaxies.

To get the masses of the stellar nuclei in the ACS Fornax Cluster Survey, we used the stellar mass-to-light (M/L) ratio versus colour index (CI), $g-z$ given by table 2 in Turner et al. (2012), relation given by Bell et al. (2003)

$$\log_{10}(M/L) = a_\lambda + b_\lambda \mathrm{CI}, \tag{1}$$

where the M/L ratio in solar units ($\mathrm{M}_\odot$) and the L above is the bolometric luminosity.

The galaxy masses for the ACSFCS sample were obtained by means of the virial theorem (Ferrarese et al. 2006a):

$$M_\mathrm{g} = \frac{\beta R_\mathrm{eff}\sigma^2}{\mathrm{G}}, \tag{2}$$

where G is the gravitational constant, σ is the galaxy velocity dispersion, R_eff is the galaxy effective radius and $\beta = 5$, as given in Ferrarese et al. (2006a). The effective radii values for the galaxies in this sample were taken from Ferguson (1989). There are no available estimates of the effective radius for the FCC 2006, FCC 1340 and FCC 21 galaxies.

The ACSVCS's nuclei masses was calculated, here again, by means of the stellar *M*/*L* ratio versus colour index formula (equation 1), and the CI used for this sample was the $g-z$, taken from Côté et al. (2006). Also in this case, the galaxy masses were obtained with equation (2). The values of the effective radii and apparent *B* magnitude for the galaxies in VCS were given in the Côté et al. (2006) catalogue.

For the NSCs in ACS, the integrated magnitudes were provided by den Brok et al. (2014) in the *F*814*W* band only, which is equivalent to the variant I_C of the *I* passband in the Johnson photometric system. Due to the absence in the den Brok et al. (2014) paper of colour index values, we decided to use the nuclei colour index average $g-z$ of the FCS and VCS samples to get the NSC masses by equation (1). The average $\overline{g-z}$ was obtained

$$\overline{g-z} = \frac{1}{2}\left(\frac{\sum_{i=1}^{N_\mathrm{FCS}}(g-z)_\mathrm{i}^\mathrm{FCS}}{N_\mathrm{FCS}} + \frac{\sum_{i=1}^{N_\mathrm{VCS}}(g-z)_\mathrm{i}^\mathrm{VCS}}{N_\mathrm{VCS}}\right), \tag{3}$$

where $g-z_\mathrm{i}^\mathrm{FCS}$ and $g-z_\mathrm{i}^\mathrm{VCS}$ are the individual $g-z$ colour indexes for Fornax and Virgo NSCs, respectively, and N_FCS and N_VCS are the numbers of objects present in the FCS and VCS samples. Of course, the assumption of a fixed value of $g-z$ for all the NSCs in the ACS sample is a limitation which hopefully will be overcome in the future. Since the authors also did not provide the values of the effective radii for the galaxies in their sample, we adopted the same procedure described above to compute the galaxies masses, i.e. calculating the colour index average value of the same previous samples mentioned, now for the galaxies, with equation (3) and applying it on equation (1).

The masses of the NSCs in *HST*/WFPC2 archive were computed by mean of equation (1) using as CI the $B-V$ found in Georgiev & Böker (2014, table 6). For the masses of galaxies in *HST* sample, due to the lack of effective radii values of the galaxies in the Georgiev & Böker (2014) work, we could not use the virial theorem (equation 2). Thus, for this sample, we adopted the same procedure used for NSC masses, i.e. we used the galaxy $B-V$ colour index given in Georgiev & Böker (2014, table 2), and evaluated M/L by equation (1). Such procedure has been already adopted in some previous work, e.g. Georgiev et al. (2016).

For the MBH data base, some values were taken from the literature such as: absolute B magnitude, velocity dispersion and masses.

Finally, the velocity dispersion values for Fornax, Virgo and *HST* samples were taken from the Hyperleda data base[1]. Matković & Guzmán (2005) and Weinzirl et al. (2014) provided the values of velocity dispersion for Coma.

3.1 Error estimates

Let us give error estimates for the various quantities discussed in this paper.

Using the standard method, we converted the galaxies apparent *B* magnitudes into absolute *B* magnitude as well as we had its errors propagated for ACSFCS, ACSVCS, ACSCCS and *HST*/WFPC2 archive. The measures of velocity dispersion for FCS, VCS and *HST*/WFPC2 and their errors can be found at the Hyperleda website (http://leda.univ-lyon1.fr). On the other hand for CCS, Matković & Guzmán (2005) used the DEDUCEME software to measure the velocity dispersion from galaxy spectra and to calculate their uncertainties. The CMOs mass errors were obtained studying the propagation of errors in each step described in the previous subsection, i.e. in equation (1). For the galaxies mass, the propagation of errors was obtained in two different ways, depending on the information given by the authors on their respective catalogues (more specific

[1] http://leda.univ-lyon1.fr/

the values of effective radii). For Fornax and Virgo clusters, we propagated the errors using the Virial formula in which the values of effective radii for their galaxies were provided. Instead for Coma Cluster and *HST*/WFPC2 archive, we propagated the galaxies mass error using the stellar M/L ratio colour–correlation formula because of the lack of effective radii values available, as reported in Section 3.

4 RESULTS

In this section, we present and discuss the possible scaling correlations for each sample described before. Such study of a large data set should lead to a better discrimination of differences between the different types of CMOs. In Table 2, we give the coefficients, a and b, of the log-linear fits to the $M_{\rm CMO}$ versus $M_{\rm B}$,σ and $M_{\rm g}$ relations, written as $\log y = a + b \log x$. These coefficients have been obtained by the non-linear least-squares Marquardt–Levenberg algorithm performing a symmetrical linear regression by minimizing the scatter on both variables x and y (Ferrarese & Merritt 2000).

In Figs 1–4, we present the $M_{\rm CMO}$ versus host galaxy $M_{\rm B}$ plots for the various data sets, whose interpolating fits are reported in Table 2. The FCS and VCS NSC samples have similar slopes (the same, within the error) and this slope is significantly steeper than those of the CCS and *HST* samples (-0.18 and -0.28, respectively). Note, also, that the exclusion from the FCS sample of the MBH and AGN points (see Fig. 1) leads to a regression fitted with a slope $b = -0.57$ instead of $b = -0.48$, which is a significant difference. The distribution of the MBH and AGN in the whole magnitude range of VCS (Fig. 2) has a slope $b = -0.53$, slightly shallower than the slope of the NSCs sub-sample, $b = -0.56$. Note also, in Fig. 2, the cut in the NSC distribution for magnitudes brighter than -18.75 in the VCS sample.

An interesting feature of Fig. 3 is the possible turndown at bright ($M_{\rm B} \leq -17$) magnitudes which can be due, as pointed out by Bekki & Graham (2010) and Arca-Sedda & Capuzzo-Dolcetta (2014), to NSC erosion by massive SMBHs present in massive galaxies. Actually, this is quantitatively supported by that the slope of the linear regression performed over galaxies fainter than $M_{\rm B} = -17$ of this sample giving a slope $b = -0.25$ significantly steeper than the one obtained over the whole $M_{\rm B}$ range (-0.18). The slope of -0.25 was also obtained when the four 'outliers' were excluded over galaxies fainter than $M_{\rm B} = -17$, being still significantly steeper

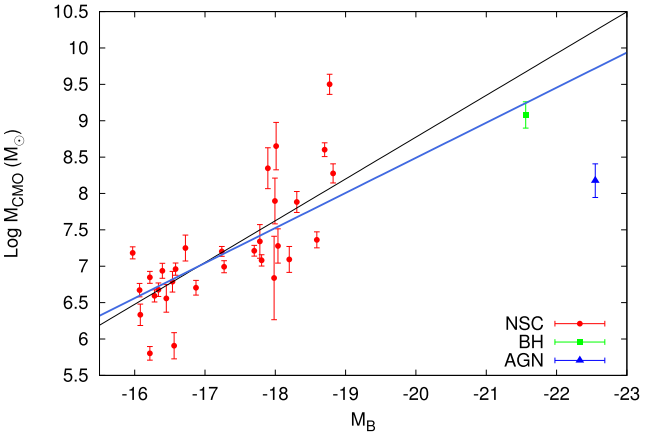

Figure 1. Masses of the NSCs of the FCS sample together with those of some BHs and AGNs in Fornax versus the integrated absolute blue magnitude of their host galaxy. The black line is the least-squares fit for only the NSCs in FCS. The blue line is the fit obtained considering NSCs, BHs and AGNs all together (see Table 2). It is clear that the cut in the NSC distribution for magnitude brighter than -18.75.

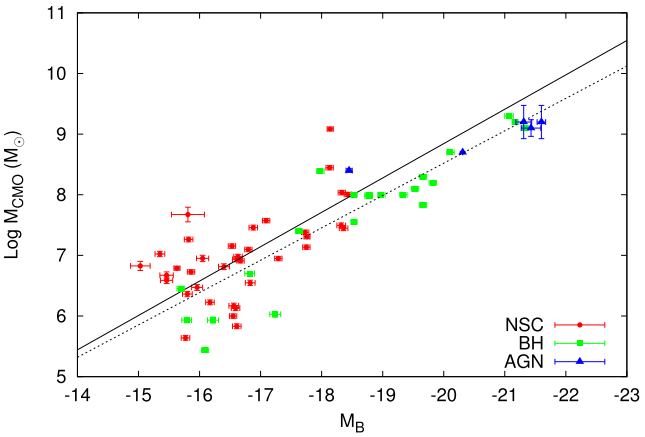

Figure 2. Masses of the NSCs of the VCS sample together with those of some BHs and AGNs in Virgo versus the integrated absolute blue magnitude of their host galaxy. The solid and dashed black lines are the least-squares fit obtained for NSCs sub-sample and for the BHs and AGNs sub-sample of the data, respectively (Table 2).

Table 2. Values of the parameters of the least-squares fit of the CMO mass versus $M_{\rm B}$, σ and $M_{\rm g}$ relations for the various data sets. The intercept a and slope b with their errors are reported. The second column specifies the CMO sub-samples for which the regressions are performed. The collection of all the NSCs of the Virgo, Fornax, Coma and *HST*/WFCP2 data sets is named here as NSC (last row in this table).

Sample	CMO type	$M_{\rm B}$ (mag)		σ (km s^{-1})		$M_{\rm g}(M_\odot)$	
		a	b	a	b	a	b
FCS	NSC	-2.71 ± 1.58	-0.57 ± 0.09	1.76 ± 1.05	3.08 ± 0.56	-3.15 ± 2.76	1.07 ± 0.28
FCS	NSC+BH+AGN	-1.15 ± 1.29	-0.48 ± 0.07	2.33 ± 0.86	2.76 ± 0.46	-1.90 ± 2.19	0.94 ± 0.22
VCS	NSC	-2.49 ± 1.69	-0.56 ± 0.10	2.69 ± 1.08	2.75 ± 0.57	-3.53 ± 2.90	1.15 ± 0.29
VCS	BH+AGN	-2.14 ± 0.76	-0.53 ± 0.03	1.94 ± 1.36	2.84 ± 0.58	-3.17 ± 1.10	1.04 ± 0.10
CCS	Entire sample	3.30 ± 0.40	-0.18 ± 0.02	1.87 ± 1.88	1.63 ± 1.19	2.15 ± 0.45	0.53 ± 0.06
CCS	No outliers and whole abscissa range	2.91 ± 0.34	-0.20 ± 0.02	–	–	1.69 ± 0.40	0.60 ± 0.05
CCS	No outliers and $M_{\rm B} \leq -17$	2.21 ± 0.49	-0.25 ± 0.03	–	–	–	–
HST	NSC	0.53 ± 0.92	-0.28 ± 0.04	2.06 ± 1.47	2.31 ± 0.79	0.84 ± 1.92	0.57 ± 0.21
HST	AGN	-1.86 ± 1.96	-0.42 ± 0.10	2.73 ± 0.43	1.89 ± 0.24	-1.61 ± 1.51	0.85 ± 0.16
MBH	BH+AGN	1.10 ± 1.40	-0.32 ± 0.07	-3.84 ± 0.66	5.19 ± 0.28	-3.13 ± 0.61	1.04 ± 0.05
NSC	NSC	1.29 ± 0.63	-0.29 ± 0.03	2.49 ± 1.16	1.84 ± 0.64	0.85 ± 0.42	0.66 ± 0.04

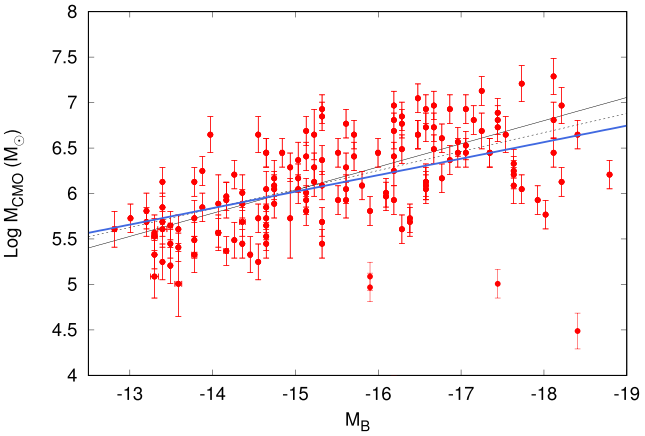

Figure 3. Masses of the NSCs of the CCS sample versus the integrated absolute blue magnitude of their host galaxy. The blue line is the least-squares fit obtained for the entire data set. The dashed black line is the regression over the whole M_B range excluding the four outlier points, and the solid black line is that limited to galaxies fainter than $M_B = -17$ and also with the outliers excluded (Table 2).

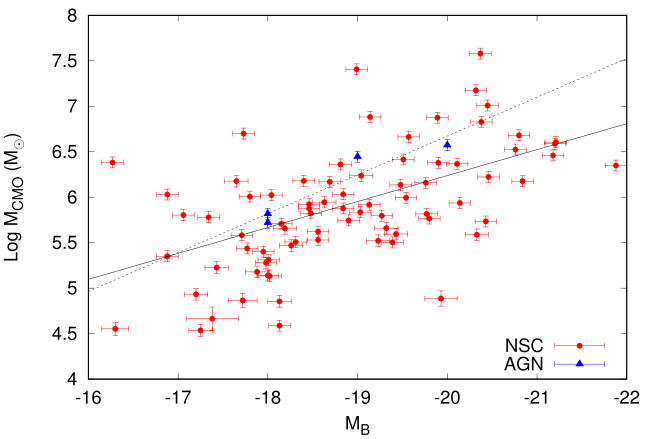

Figure 4. Masses of the NSCs of the *HST* sample together with those of some AGNs of the *HST*/WFCP2 archive versus the integrated absolute blue magnitude of their host galaxy. The black solid line is the least-squares fit for the NSCs and the dashed black line is that for the AGNs in the data (Table 2).

than the one obtained over the whole M_B range and excluding the 'outliers', $b = -0.20$.

This flattening at high host luminosities is also present in Fig. 4 (*HST* sample), well represented by the black solid line, while it is not visible in Figs 1 and 2 (FCS and VCS) because of the low sample abundance which implies a sort of cut-off in the NSC distribution at host magnitudes brighter than $M_B \simeq -19$. To check the influence of the (few) AGNs in this *HST* sample, we separated data in two sub-samples, one for NSCs and one for AGNs. If we perform the fit over the galaxies hosting AGNs, which corresponds to magnitudes brighter than -18, the slope obtained is $b = -0.42$, significantly steeper than the one obtained considering just the NSC sub-sample, $b = -0.28$. This result has, anyway, a weak statistical relevance because the number of AGNs is just 8 vesrus 220 NSCs.

The M_{CMO} versus M_g relations are shown in Figs 5–8. Note that also for the FCS sample (Fig. 5), the inclusion or the exclusion of the MBH and AGN causes a significant change in the slope of the regression fits, from $b = 0.94$ (blue line) including them to $b = 1.07$ excluding them (black line). For the VCS (Fig. 6), where the number

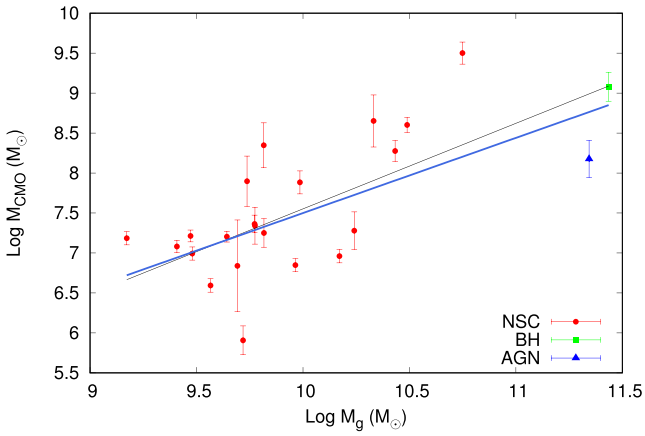

Figure 5. Masses of the NSCs of the FCS sample together with those of some BHs and AGNs in Fornax versus their host galaxy mass. The black line is the least-squares fit for only the NSCs in the FCS sample. The blue line is obtained by fitting NSCs, BH and AGN all together (see Table 2).

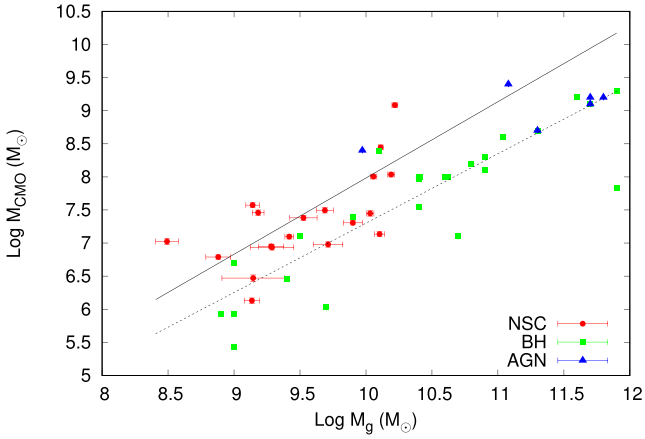

Figure 6. Masses of the NSCs of the VCS sample together with those of some BHs and AGNs in Virgo versus their host galaxy mass. The solid and dashed black lines are the least-squares fit obtained for NSCs sub-sample and for the BHs and AGNs sub-sample of the data, respectively (Table 2).

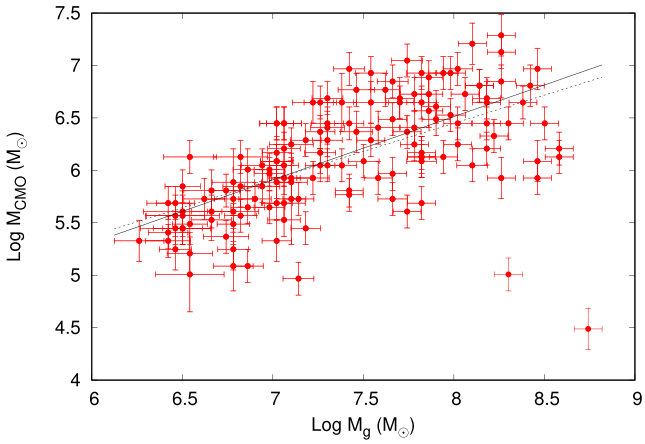

Figure 7. Masses of the NSCs of the CCS sample versus their host galaxies masses. The black dashed line is the least-squares fit obtained for the entire data set and the solid black line is the fit obtained excluding the two lightest NSCs in the sample (Table 2).

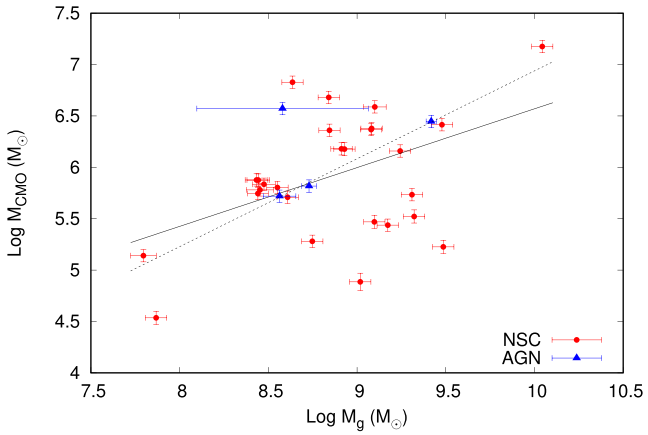

Figure 8. Masses of the NSCs of the *HST* sample together with those of some AGNs of the *HST*/WFCP2 archive versus their host galaxy mass. The black solid line is the least-squares fit for the NSCs, only, and the dashed black line is the fit for the AGNs (Table 2).

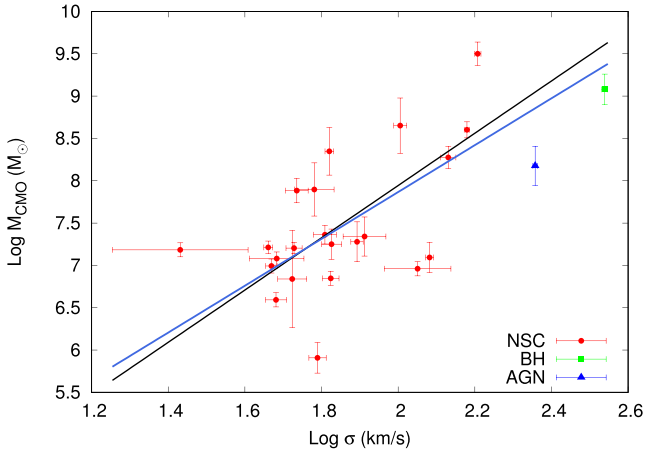

Figure 9. Masses of the NSCs of the FCS sample together with that of a BH and an AGN in Fornax versus the velocity dispersion of their host galaxy. The black line is the least-squares fit for only the NSCs in FCS. The blue line is the least-squares fit obtained considering NSCs, BH and AGN all together (Table 2).

of MBHs and AGNs is abundant enough to draw some conclusions, we see that the regression fit for the NSCs sub-sample and that for the MBH/AGN sub-sample show a significant difference. In the CCS sample (Fig. 7), where we have no MBH and AGN, we did not identify and excluded any outliers, obtaining a slope of $b = 0.53$. Note, anyway, the presence of two very light NSCs in relatively massive galaxy hosts (the two data points in the bottom right part of the figure, clearly 'separated' from the rest of the distribution). Excluding them from the sample, the slope increases to $b = 0.60$. In the *HST* sample (Fig. 8), the AGNs have a steeper slope, $b = 0.85$ than the one, $b = 0.57$, found for the NSCs.

Figs 9–12 refer to the M_{CMO} versus σ relations. The weight of the BH and the AGN data points in the FCS also changed the regression fit for this scaling relation as shown in Fig. 9, $b = 2.76$, when including them, against 3.08 when excluding them. The slopes obtained for the VCS NSCs ($b = 2.75$) and MBH/AGN ($b = 2.84$) sub-samples (Fig. 10) do not show significant difference, even with the clear cut in the NSC distribution for $\log\sigma \lessapprox 1.8$. The σ values for CCS show a very huge scatter in Fig. 11, which cause the lowest slope of the entire data set, $b = 1.63$. For the *HST*/WFPC2

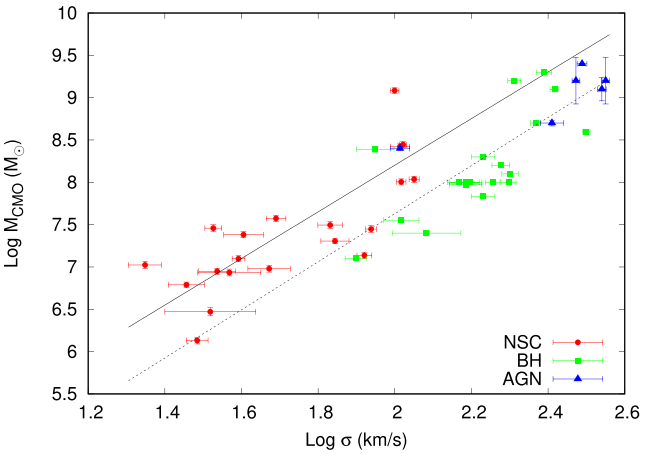

Figure 10. Masses of the NSCs of the VCS sample together with BHs and AGNs in galaxies of the Virgo cluster versus the velocity dispersion of their host galaxy. The solid and dashed black lines are the least-squares fit obtained for NSCs sub-sample and for the BHs and AGNs sub-samples, respectively (Table 2).

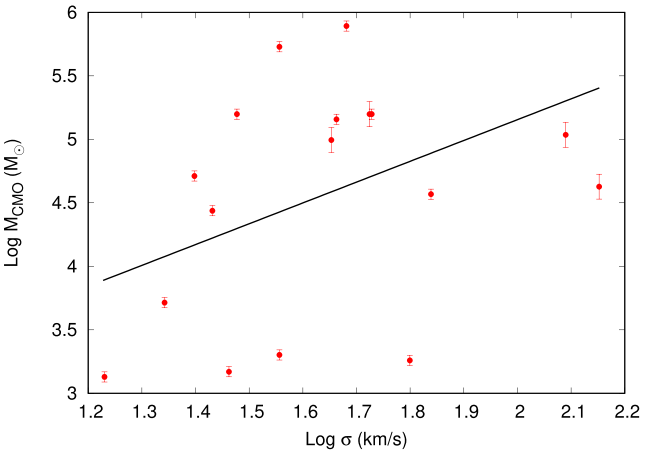

Figure 11. Masses of the NSCs of the CCS sample versus the velocity dispersion of their host galaxy. The black line is the least-squares fit to the data (Table 2).

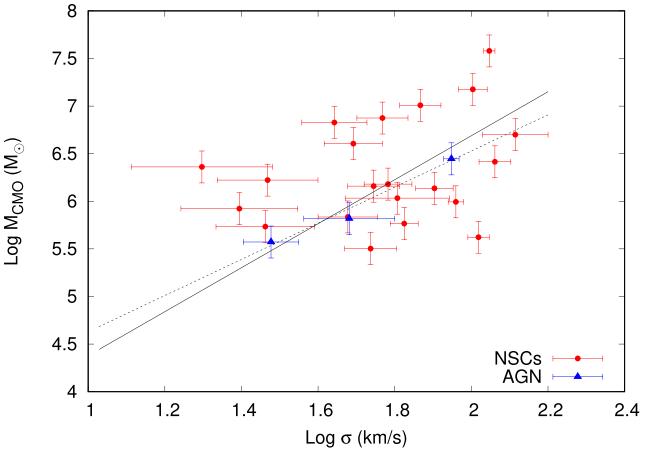

Figure 12. Masses of the NSCs of the *HST* sample together with those of some AGNs of the *HST*/WFCP2 archive versus the velocity dispersion of their host galaxy. The black solid line is the least-squares fit for the NSCs and the dashed black line is the fit for the AGNs in the data set (Table 2).

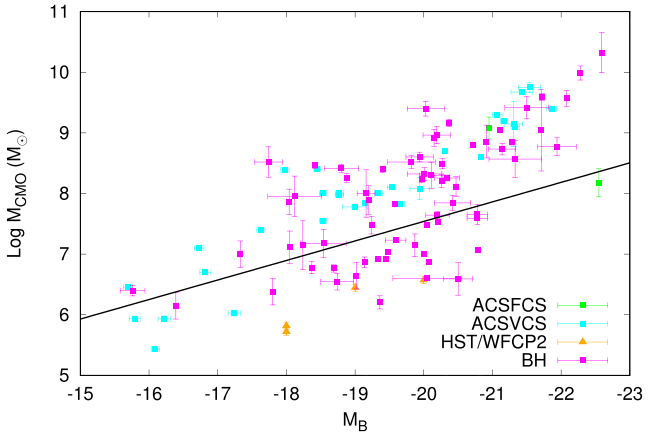

Figure 13. Masses of the whole BH sample plotted against absolute blue magnitude of the host galaxy. The green squares are the BH and the AGN present in ACSFCS. The cyan squares are the BHs and AGNs present in ACSVCS. The AGNs in *HST*/WFPC2 are shown as orange triangles. The magenta squares are the new collection of BHs. The black line shows the best fits to this sample and its values are presented in Table 2.

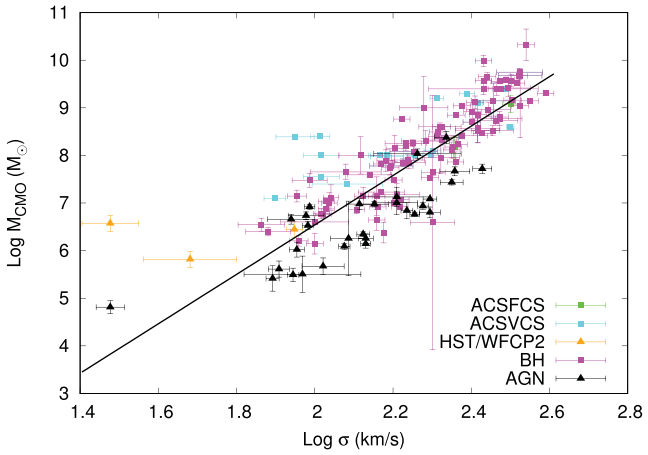

Figure 14. Masses of the whole BH sample plotted against velocity dispersion σ of the host galaxy. The green squares are the BH and the AGN present in ACSFCS. The cyan squares are the BHs and AGNs present in ACSVCS. AGNs in *HST*/WFPC2 are shown as orange triangles. The new collections of BHs and AGNs are the magenta squares and the black triangles, respectively. The black line shows the best fits to this sample and its values are presented in Table 2.

archive (Fig. 12), the slopes found for the AGNs sub-sample and the one found for the NSCs sub-sample are significantly different, $b_{\rm agn} = 1.89$ and $b_{\rm nsc} = 2.31$, due, likely, to the low number of AGNs in this sample.

The scaling relations for the MBH sample mass with various properties of their host galaxies are presented in Figs 13–15. Figs 13–15 show the $M_{\rm MBH} - M_{\rm B}$, $M_{\rm MBH} - M_{\sigma}$ and $M_{\rm MBH} - M_{\rm g}$ relations, respectively. We gave particular attention to deducing the $M_{\rm MBH}$–σ fitting relation in Fig. 14. As reported by Graham et al. (2011), a modified regression analysis is required to correct the sample bias problem in galaxies which their central black holes/AGNs have masses $\leq 10^6$ solar masses, applied here for the AGNs inside our MBH sample. In our MBH sample, if we do not consider the sample bias correction for the AGNs, we get a slope of 4.30, which is not in agreement with the most recent findings Graham et al. (2011) and Graham (2012). If, instead, we consider the bias

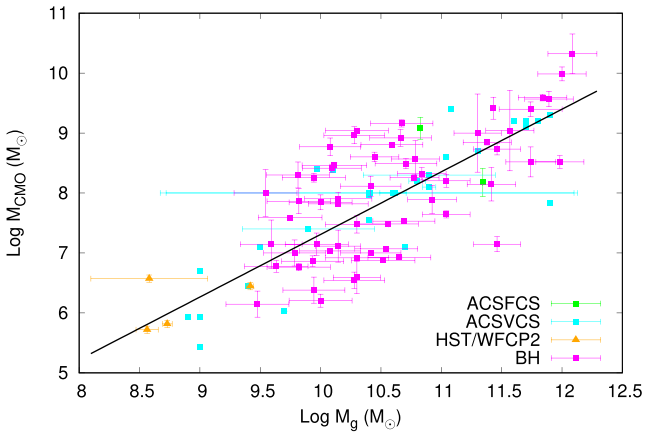

Figure 15. Masses of the whole BH sample plotted against the mass of the host galaxy.

correction, following the values presented by Graham et al. (2011, table 3), for the galaxies with AGNs of low masses we get a larger slope ($b = 5.19$). This result is in better agreement with the most recent results. The direct implication of such correction is a change of the offset behaviour in the $M_{\rm MBH}$–σ plot of which move galaxies below or rightward of the upper envelope of points in the diagram (Graham et al. 2011).

4.1 Comparative discussion

The possible existence of scaling relations indicates a direct link between large galactic spatial scales and the nuclear environment, being an important clue to the understanding the mechanisms behind the CMO formation.

Some studies in the literature have shown that the correlations between NSCs and their host galaxies follow, at least in part, a behaviour similar to those of MBHs (Rossa et al. 2006). In spite of these hints of similarity, it is still unclear what the two types of CMOs have in common, and what, possibly, links the central galactic BH and NSC growth and evolution. Some more light on this topic could be given by the study of a more extended data base, which must be collected in the ample literature.

Actually, in the following subsections, we present the $M_{\rm CMO}$ versus $M_{\rm B}$, galaxies masses and σ relations with the most abundant set of data we could gather from already published data. By means of the approach presented above, we were able to fit bilogarithmic functions for the relations among the CMOs masses and various parameters characterizing their host galaxies, as summarized in Table 2.

4.1.1 CMO mass versus $M_{\rm B}$ and M_g

The presence of NSCs in faint galaxies, with magnitudes between $-19 \leq M_{\rm B} \leq -13$, is more common than in brighter galaxies as shown in Fig. 16. This was noted first by Côté et al. (2006): as galaxies become fainter, the presence of NSC becomes a more common feature. On the other hand, galaxies brighter than $M_{\rm B} \leq -19$ almost always host MBHs, and the existence of such objects in bright galaxies reconcile with the existence, in most of the cases, of an AGN. It is well known that GCs in dwarf galaxies are, on average, less luminous than those associated with giant galaxies. Thus, the dearth of NSCs in faint galaxies could be related to the small number of GCs that may not be clearly distinct in some dwarf

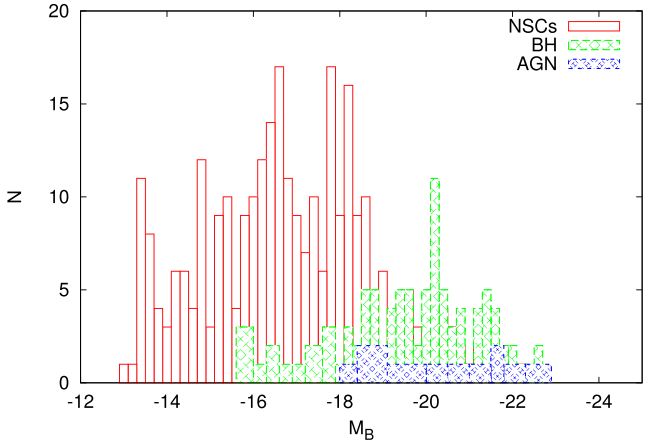

Figure 16. Distribution of all the CMOs belonging to the ACSFCS, ACSVCS, ACSCCS, *HST*/WFCP2 archive and the MBH sample.

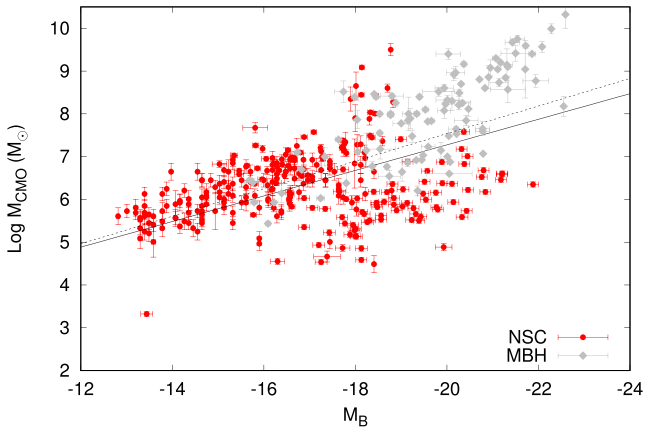

Figure 17. CMOs masses versus the absolute B magnitude of the host galaxies. The black solid line and the black dotted line are the best fits for MBH and NSC samples, respectively (Table 2).

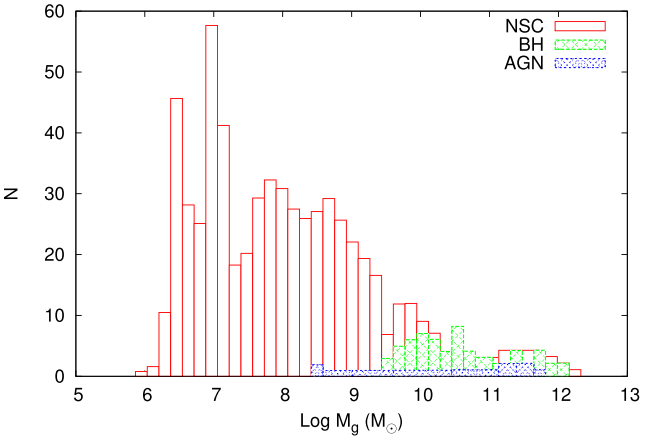

Figure 18. Distribution of the host galaxy masses of whole NSC sample and of MBH+AGN sample.

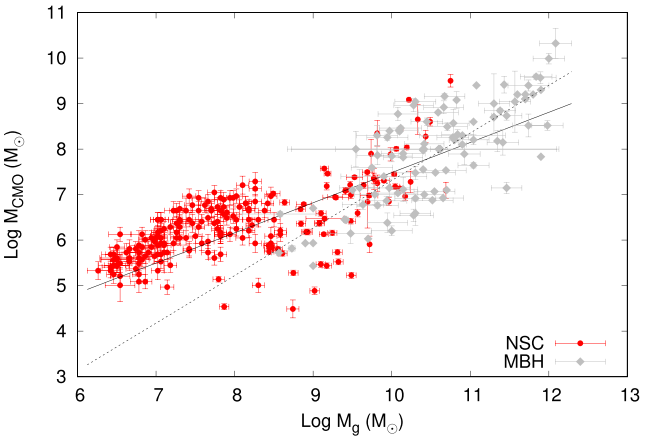

Figure 19. CMO masses versus the mass of the host galaxies. Solid line is the fit to MBH data, dotted line to NSC (Table 2).

galaxies, as for example NGC 5128 in which there is not a clear-cut dichotomy among them (van den Bergh 2007).

Fig. 17shows the comparison between NSCs and MBHs masses plotted versus their host galaxy M_B in our whole data sample. The slopes of the M_{MBH}–M_B and of the M_{NSC}–M_B relations are the same, within their errors.

CMOs are present in all galaxies of our sample, as we move for the bright galaxies range we can see that somehow the NSCs may be destroyed by the pre-existing MBH, or they may collapse into the galaxy central region and form a powerful object as an AGN, resulting in the dominance of those massive objects in such range. At this regard as suggested first by Capuzzo-Dolcetta (1993), a very dense star cluster could have formed in the centre of a galaxy in its first Gyr of life inducing a BH seed growth therein. Another hypothesis for the clear depauperation of NSCs in galaxies brighter than −19, as well as the clear flattening of the NSC mass versus host galaxy integrated magnitude and mass, as shown in Fig. 17, can be related to the formation of giant ellipticals through merging of smaller galaxies as suggested by Merritt (2006). It is still unclear which process drives the dominance of one type of object or another and more studies are needed about this matter.

We essentially reconfirm the Ferrarese et al. (2006a) finding with our extended and updated set of data: as one moves to fainter galaxies, the stellar nuclei become the dominant feature, while a more massive object tend to become less common and, perhaps, to entirely disappear at the fainter end.

On the other side, galaxies with larger mass have more massive CMOs in their centres, in the form of MBH or/and an AGN (Fig. 18). The lack of galaxies with mass below 10^9 $M_\odot$ containing an MBH in their centre is evident and likely due to the fact that such (relatively light) MBHs are not easily detected with current instruments and/or analysis techniques. In the nuclei of intermediate-mass galaxies (between 10^8 and 10^{11} $M_\odot$), the coexistence of both MBHs and NSCs is not clear, as well as the reason for the dominance of one or the other. In galaxies with higher masses ($\geq 10^{11}$ $M_\odot$), NSCs are rare; a possible explanation for this is that in massive galaxies some physical process connected with the presence of an MBH and/or AGN inhibits the formation and destroys a central NSC. One possible explanation of such physical process was reported in Bekki & Graham (2010) simulations, where if two galaxies hosting MBHs collides, a black hole binary could form heating up the stellar nucleus causing its progressive evaporation and, consequently, its destruction. Another explanation is that of the strong combined SMBH+galaxy tidal disturbance in massive galaxies (Arca-Sedda, Capuzzo-Dolcetta & Spera 2017).

The best-fitting relations of M_{NSC} and M_{MBH} versus M_g are shown in Fig. 19. This figure shows a clear difference between the slopes of the fitting functions for the two sub-samples, the M_{MBH} versus M_g relation being much steeper ($b = 1.05$) than the one for M_{NSC}

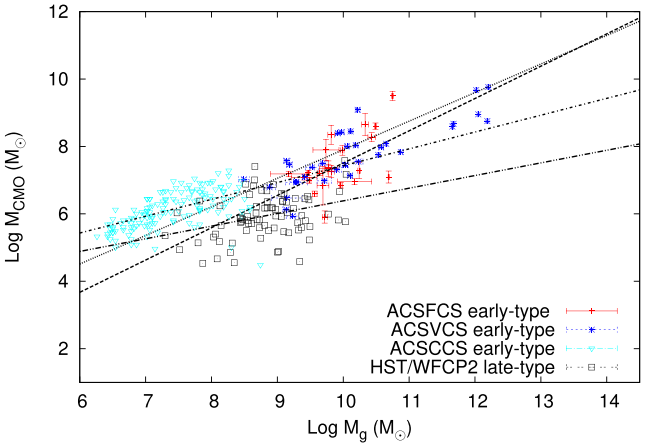

Figure 20. Masses of the CMOs versus the mass of the host galaxies.

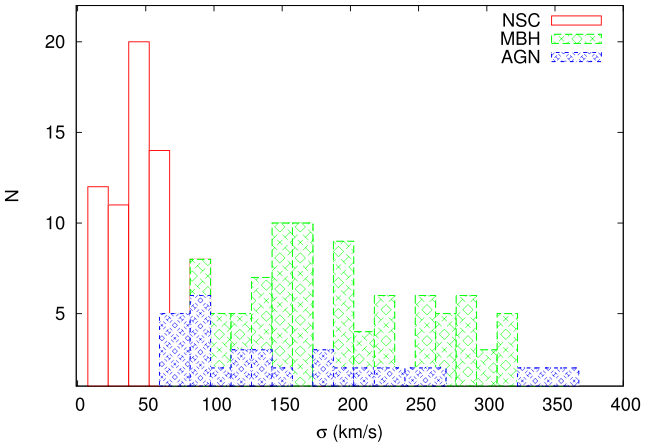

Figure 21. Distribution of all the CMOs belonging to the ACSFCS, ACSVCS, *HST*/WFCP2 archive, ACSCCS and MBH sample.

($b = 0.66$). The difference is also in the mass range covered by the hosts, as reflected by the M_g histogram in Fig. 18.

It is also relevant noting that the slope of ∼0.66 for the M_{NSC}–M_g relations is compatible with the findings presented by Scott & Graham (2013), which are corroborated here by a much larger sample. Also the slope for the M_{MBH}–M_g relation (1.05 ± 0.05) is compatible with those reported in the literature (Häring & Rix 2004), giving an almost linear (slope ∼1) scaling.

We also found different slopes values for different galaxy types (early or late-type), as depicted in Fig. 20. The slope for early-type galaxies is steeper than for late-type galaxies, and this behaviour might be caused by an overestimate of NSC masses. The agitated merger history of the hosts in early-type galaxies leads the growth of their NSCs by funnelling material into its centre. On the other hand, late-type galaxies have not experienced a significant merger, leading to a proportional growth of either nucleus o host mass, resulting in a shallower slope (Georgiev et al. 2016).

4.1.2 CMO mass versus σ

The correlation between the CMOs masses and the host galaxy velocity dispersion is one of the most interesting relations to analyse because it evidences a possible physical difference between NSCs and MBHs. The histogram in Fig. 21 indicates a separation between the two classes of objects: NSCs are frequent in low σ (low mass) hosts, while MBHs are present mainly in high σ (massive) hosts. The results found here for the M_{CMOs}–σ relation are consistent with those presented in Robertson et al. (2006), which suggest that as σ increases denser structures are found, either MBHs or AGNs. There is also a range of galaxy velocity dispersion where the largest numbers of CMOs (NSCs and MBH) are found: in galaxies with $50 \leq \sigma \leq 100\,\mathrm{km\,s^{-1}}$.

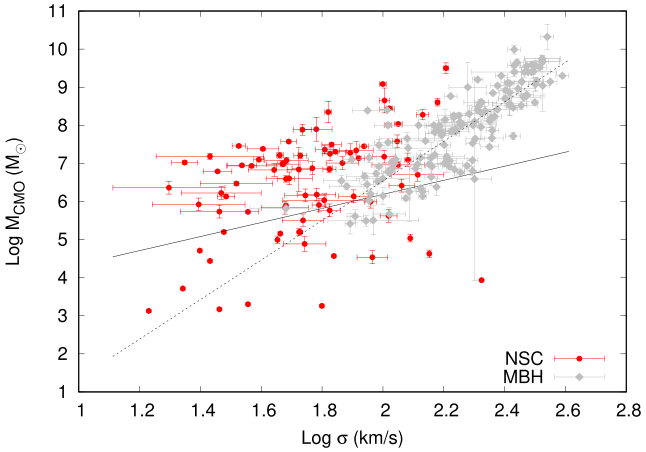

Figure 22. CMOs masses versus the velocity dispersion σ of the host galaxies.

In Fig. 22, we can see a significant difference in the slope of the M_{NSC}–σ relation and that of the M_{MBH}–σ relation, the first being smaller. Since the studies of Gebhardt et al. (2000) and Ferrarese & Merritt (2000), the slopes for the M_{CMOs}–σ relation have received great attention. While Ferrarese et al. (2006a) showed that the relation of NSC mass versus the host galaxy velocity dispersion is roughly the same observed for MBHs, Graham (2012) claimed that the M_{NSC}–σ relation is much shallower (in a range 1.52–3) than for MBHs. A small slope in the M_{NSC}–σ relation is fully compatible with the scenario of NSC formation by GC merger as discussed in the following subsection. Our results point towards a weak scaling of this relation, with a slope of $b = 1.84$, fitting well the dry merger scenario.

At the same time, the M_{MBH}–σ relation has also received attention over, since Gebhardt et al. (2000) reported a slope of 3.75 for it. After that others values for the slopes have been reported by different authors depending, of course, on the approach and how they treated their different sets of data, until Scott & Graham (2013), who reported a slope of 5–6 for the M_{MBH}–σ relation.

Following such tendency here, we present our result with an even larger data set. Our final result points a slope for the M_{MBH}–σ relation slightly greater than 5 ($b = 5.19$), consistent with previous results reported (Graham 2012; Scott & Graham 2013).

The slope of the M_{MBH}–σ relation for the full galaxy sample is even steeper (between 5 and 6, Graham 2012), if we focus our attention to MBHs in the high-mass tail of the host distribution. The slope $b = 5.19$ for our sample is explained by: (i) the inclusion of galaxies hosting either BHs or AGNs with low mass ($\sim \leq 10^6\,M_\odot$), having also low velocity dispersion σ, values of σ comparable with those galaxies hosting NSCs, i.e. in the range between $1.6 \leq \sigma \leq 3.0$ and (ii) a potential sample bias for the galaxies with a low central mass AGNs. The apparent lack of systems with BH and/or AGNs in galaxies whose σ are below 100 km s^{-1} is noteworthy, confirming that higher velocity galaxies harbour more massive objects in their centre.

4.2 Theoretical interpretation of the NSC mass versus σ relation

As we saw above, in our sample the slope of the $M_{\rm NSC}$ versus σ correlation is significantly smaller than that of the MBH.

Intriguingly, this shallower profile has a straightforward interpretation in the infall and merger scenario for NSC formation. This has been already studied by Capuzzo-Dolcetta (1993), Antonini (2013) and Arca-Sedda & Capuzzo-Dolcetta (2014) and here we will extend their analysis of the NSC mass–σ correlation.

Actually, a shallow dependence of the NSC mass on σ is a natural output of the dynamical friction induced infall of GC towards the host galaxy centre. This is seen by the following, simple, formal argument. Following the derivation in Arca-Sedda & Capuzzo-Dolcetta (2014), based on the assumption of GCs of equal mass M, spatially distributed according to a spherical mass density power law $\rho(r) \propto r^{\alpha}$ in a singular isothermal spherical galaxy ($\rho_{\rm g}(r) \propto r^{-2}$) with mass $M_{\rm g}$, constant velocity dispersion σ and spatially cut at R, the nucleus mass resulting from GC merger is, at every time t

$$M_{\rm n} = f\frac{2}{\rm G}(0.6047{\rm G}\ln\Lambda M)^{\alpha+3}t^{\frac{\alpha+3}{2}}\frac{\sigma^{\frac{1-\alpha}{2}}}{R^{\alpha+2}}, \quad (4)$$

for $t \leq \sigma R_0^2/(0.6047{\rm G}\ln\Lambda M)$, while $M_{\rm n}(t)$ saturates to $M_{\rm GCS}$ at $t = \sigma R_0^2/(0.6047{\rm G}\ln\Lambda M)$.

Equation (4) (in which $f < 1$ is the fraction of the total GC mass to the galactic mass) is obtained by a straightforward analytical integration of the first-order differential equation governing the orbital angular momentum evolution of the GC in the host galaxy. Note that equation (4) reduces to the $M_{\rm n}$–σ scaling relation, $M_{\rm n} \propto \sigma^{3/2}$, already obtained by Tremaine, Ostriker & Spitzer (2012) in the case of $\alpha = -2$, i.e. for GCs distributed the same way as the galactic isothermal background.

This is the only case where the explicit dependence on the galactic radius R cancels out. Note also that for $\alpha = -2$, the NSC mass should scale, in a sample of galaxies of same size R, as $M_{\rm g}^{3/4}$, assuming a virial link among σ, $M_{\rm g}$ and R.

For a generic α, the last fraction (depending on σ and R) in equation (4) is $M_{\rm g}^{\frac{1-\alpha}{4}}/R^{\frac{3\alpha+3}{4}}$, which reduces to the above for $\alpha = -2$.

For other values of α in the allowed range, the dependence of $M_{\rm n}$ on σ, in the assumption of a virial relation between galactic R and $M_{\rm g}$ ($R \propto M_{\rm g}/\sigma^2$), becomes

$$M_{\rm n}(t) \propto \frac{\sigma^{\frac{9+3\alpha}{2}}}{M_{\rm g}}, \quad (5)$$

which corresponds to a slope in the range from 0 of the steeper ($\alpha = -3$) GCS radial distribution to 9/2 of the flat ($\alpha = 0$) distribution.

The relevant result here is that the slope of the $M_{\rm n}$–σ relation in the regime of dynamical friction dominated infall process is expected to have an upper bound which is in any case smaller than that of the $M_{\rm BH}$–σ relation. This seems a strong support to the infall and merger scenario of NSC formation.

5 SUMMARY AND CONCLUSIONS

In this paper, we compiled the largest set of possible reliable data available in the literature in order to study possible correlations among CMO masses and properties of their parent galaxies. Our collection of data in digital form is available upon request to the authors. We also made a thorough comparison of NSC and MBH relations and found evidence of a significant difference between the two sets, thing that still deserves a convincing physical explanation.

A summary of our findings is:

(i) the slopes we find for the $M_{\rm NSC}$–$M_{\rm B}$ relation in our huge data set, $-0.57 \leq b \leq -0.20$, are very similar to those obtained by Ferrarese et al. (2006a);

(ii) the distributions of the masses of NSCs and that of MBH as a function of the host galaxy integrated B magnitude are different in what NSCs cover a range of lower host luminosities and they quite clearly show a closer correlation at lower luminosities than at brighter, where the mass–$M_{\rm B}$ correlation flattens out; MBH are present also in very bright galaxies;

(iii) the relation $M_{\rm CMO}$–$M_{\rm g}$ ($M_{\rm g}$ is the host galaxy mass) shows a steeper slope for the early-type galaxies data set, i.e. FCS, VCS and CCS, than for the late-type galaxies data set, i.e. *HST*/WFCP2 archive, in good agreement with recent results presented by Georgiev et al. (2016);

(iv) we give a further strong evidence that NSCs are more frequently found in galaxies with low σ and small $M_{\rm g}$, while BHs and AGNs are more common in galaxies with high σ and large $M_{\rm g}$;

(v) the scaling of $M_{\rm MBH}$ with $M_{\rm g}$ is almost linear, $b = 1.05 \pm 0.05$, in good compatibility with those in the literature, i.e. Häring & Rix (2004);

(vi) the slope we obtain for the MBH mass–velocity dispersion relation, $b = 5.19 \pm 0.28$, is in good agreement with the most recent findings by Graham (2012), although we added here a large number of galaxies hosting either BHs or AGNs with low mass and σ, whose presence yields to a shallower slope;

(vii) on the other side, our results indicate a much weaker scaling of $M_{\rm NSC}$ versus σ, with slopes in the range 2–3 over the various sets of data examined here, in very good agreement with the GC infall and merger scenario for the NSC formation (Capuzzo-Dolcetta 1993; Tremaine et al. 2012; Antonini 2013; Arca-Sedda & Capuzzo-Dolcetta 2014).

ACKNOWLEDGEMENTS

ITM is supported by CAPES-Brazil through the grant 9467/13-0. Part of this work was performed at the Aspen Center for Physics, which is supported by National Science Foundation grant PHY-1066293. At this regard, RCD thanks the Simons foundation for the grant which allowed him a period of stay at the Aspen Center for Physics where he developed part of this work. We thank Dr. A. Graham for his useful suggestions during the preparation of the manuscript. We also thank Dr. D. Cole who helped us to improve the paper and correct some inconsistencies.

REFERENCES

Antonini F., 2013, ApJ, 763, 62
Arca-Sedda M., Capuzzo-Dolcetta R., 2014, MNRAS, 444, 3738
Arca-Sedda M., Capuzzo-Dolcetta R., Spera M., 2017, MNRAS, 456, 2457
Balcells M., Graham A. W., Domínguez-Palmero L., Peletier R. F., 2003, ApJ, 582, L79
Baldassare V. F., Reines A. E., Gallo E., Greene J. E., 2015, ApJ, 809, L14
Bekki K., Graham A. W., 2010, ApJ, 714, L313
Bell E. F., McIntosh D. H., Katz N., Weinberg M. D., 2003, ApJS, 149, 289
Böker T., van der Marel R. P., Mazzuca L., Rix H.-W., Rudnick G., Ho L. C., Shields J. C., 2001, AJ, 121, 1473
Capuzzo-Dolcetta R., 1993, ApJ, 415, 616
Carson D. J., Barth A. J., Seth A. C., den Brok M., Cappellari M., Greene J. E., Ho L. C., Neumayer N., 2015, AJ, 149, 170
Côté P. et al., 2006, ApJS, 165, 57
den Brok M. et al., 2014, MNRAS, 445, 2385

Erwin P., Gadotti D. A., 2012, Adv. Astron., 2012, 946368
Ferguson H. C., 1989, AJ, 98, 367
Ferrarese L., Ford H., 2005, Space Sci. Rev., 116, 523
Ferrarese L., Merritt D., 2000, ApJ, 539, L9
Ferrarese L. et al., 2006a, ApJS, 164, 334
Ferrarese L. et al., 2006b, ApJ, 644, L21
Gallo E., Treu T., Jacob J., Woo J.-H., Marshall P. J., Antonucci R., 2008, ApJ, 680, 154
Gebhardt K. et al., 2000, ApJ, 539, L13
Georgiev I. Y., Böker T., 2014, MNRAS, 441, 3570
Georgiev I. Y., Böker T., Leigh N., Lützgendorf N., Neumayer N., 2016, MNRAS, 457, 2122
Graham A. W., 2012, MNRAS, 422, 1586
Graham A. W., Guzmán R., 2003, AJ, 125, 2936
Graham A. W., Spitler L. R., 2009, MNRAS, 397, 2148
Graham A. W., Erwin P., Caon N., Trujillo I., 2001, ApJ, 563, L11
Graham A. W., Onken C. A., Athanassoula E., Combes F., 2011, MNRAS, 412, 2211
Graham A. W., Ciambur B. C., Soria R., 2016, ApJ, 818, 172
Greene J. E., Ho L. C., 2006, ApJ, 641, L21
Häring N., Rix H.-W., 2004, ApJ, 604, L89
Hu J., 2008, MNRAS, 386, 2242
Kormendy J., McClure R. D., 1993, AJ, 105, 1793
Kormendy J., Richstone D., 1995, ARA&A, 33, 581
Matković A., Guzmán R., 2005, MNRAS, 362, 289
Merritt D., 2006, Rep. Prog. Phys., 69, 2513
Neumayer N., 2015, in Montmerle T., ed., IAU Symp. 10, Origin and Complexity of Massive Star Clusters. Kluwer, Dordrecht, p. 262
Nowak N., Saglia R. P., Thomas J., Bender R., Davies R. I., Gebhardt K., 2008, MNRAS, 391, 1629
Peng C. Y., 2007, ApJ, 671, 1098
Peterson B. M. et al., 2004, ApJ, 613, 682
Robertson B., Hernquist L., Cox T. J., Di Matteo T., Hopkins P. F., Martini P., Springel V., 2006, ApJ, 641, 90
Rossa J., van der Marel R. P., Böker T., Gerssen J., Ho L. C., Rix H.-W., Shields J. C., Walcher C.-J., 2006, AJ, 132, 1074
Savorgnan G. A. D., Graham A. W., 2015, MNRAS, 446, 2330
Savorgnan G. A. D., Graham A. W., 2016, ApJS, 222, 10
Savorgnan G. A. D., Graham A. W., Marconi A., Sani A., 2016, ApJ, 817, 21
Schödel R., Merritt D., Eckart A., 2009, A&A, 502, 91
Scott N., Graham A. W., 2013, ApJ, 763, 76
Seth A., Agüeros M., Lee D., Basu-Zych A., 2008, ApJ, 678, 116
Tremaine S. D., Ostriker J. P., Spitzer L., Jr, 1975, ApJ, 196, 407
Turner M. L., Côté P., Ferrarese L., Jordán A., Blakeslee J. P., Mei S., Peng E. W., West M. J., 2012, ApJS, 203, 5
van den Bergh S., 2007, AJ, 133, 1217
Wehner E. H., Harris W. E., 2006, ApJ, 644, L17
Weinzirl T. et al., 2014, MNRAS, 441, 3083
Windhorst R. A. et al., 1991, ApJ, 380, 362

This paper has been typeset from a TEX/LATEX file prepared by the author.